

Hybrid density functional calculations of the band gap of $\text{Ga}_x\text{In}_{1-x}\text{N}$

Xifan Wu¹, Eric J. Walter², Andrew M. Rappe³, Roberto Car¹, and Annabella Selloni¹

¹Chemistry Department, Princeton University, Princeton, NJ 08544-0001, USA

²Department of Physics, College of William and Mary, Williamsburg, Virginia 23187-8795, USA and

³The Makineni Theoretical Laboratories, Department of Chemistry, University of Pennsylvania, Philadelphia, Pennsylvania 19104-6323, USA

(Dated: October 23, 2018)

Recent theoretical work has provided evidence that hybrid functionals, which include a fraction of exact (Hartree Fock) exchange in the density functional theory (DFT) exchange and correlation terms, significantly improve the description of band gaps of semiconductors compared with local and semilocal approximations. Based on a recently developed order- N method for calculating the exact exchange in extended insulating systems, we have implemented an efficient scheme to determine the hybrid functional band gap. We use this scheme to study the band gap and other electronic properties of the ternary compound $\text{In}_{1-x}\text{Ga}_x\text{N}$ using a 64-atom supercell model.

PACS numbers: 71.15.DX, 71.15.Mb, 71.20.Nr

The design of novel functional semiconductors with given values of the energy band gap is an area of intense research^{1,2,3,4,5}. In particular, much attention is focused on the band gap engineering of group-III nitride semiconductors, whose remarkable optical properties are important for optoelectronic device applications^{6,7}. To guide the search for compounds with tailored properties¹, experimental studies are often accompanied by electronic structure calculations based on density functional theory (DFT)⁸. For these calculations, the local-density(LDA) or generalized gradient approximations(GGA) are typically used. Due to the delocalization error of the LDA and GGA exchange and correlation functionals, however, these approaches severely underestimate the materials band gaps^{9,10}.

As shown by several recent studies¹¹, a significant improvement in the description of semiconductor and insulator band gaps is generally obtained by using hybrid functionals¹², in which some exact (Hartree-Fock) exchange is mixed into the exchange and correlation functional. This reduces the delocalization and derivative discontinuity errors of (semi)local functionals^{2,9,10,11}. However, because of the considerable computational cost of evaluating the non-local exact exchange term, hybrid functionals have been mostly applied to systems with small unit cells¹³. For the modeling of systems where a large supercell is needed, an additional screened exchange approximation is usually made to relieve the computational burden^{2,11}.

Recently Wu *et al.* (WSC)¹⁴ introduced an order- N method to calculate the exact exchange in extended insulating systems. The WSC method is based on a localized Wannier function representation of the occupied (valence) space, so that the exchange interaction between two orbitals decays rapidly with the distance between their centers. A truncation can thus be introduced, which greatly reduces the computational cost. The effectiveness of the WSC method was demonstrated by ground state electronic minimizations for crystalline silicon in supercells with 64 and 216 atoms.

In this paper, we extend the WSC scheme to compute hybrid functional band gaps. To this end, the system's first (few) empty conduction state(s) is(are) determined starting from the ground state calculated via the WSC method. With hybrid functionals, this requires the computation of the pair exchange between the empty state and each valence orbital. Even though the empty state is delocalized, the product between this state and a valence orbital is well localized, so that the corresponding exchange interaction can be truncated as in the original WSC method¹⁴. We apply our scheme to determine the band gap of $\text{In}_{1-x}\text{Ga}_x\text{N}$, a ternary nitride semiconductor of great technological interest, and of its parent compounds, InN and GaN, using the PBE0 hybrid functional¹⁶. Our results show that, compared to the semi-local PBE functional, PBE0 gives a considerably improved description of the band gap, as well as of the cation d state binding energy, which is also poorly described by the semilocal functionals.

The PBE0 hybrid functional is constructed by mixing 25% of exact exchange with the GGA-PBE exchange¹⁶, while the correlation potential is still represented by the corresponding functional in PBE¹⁷,

$$E_{xc}^{\text{PBE0}} = \frac{1}{4}E_x + \frac{3}{4}E_x^{\text{PBE}} + E_c^{\text{PBE}}. \quad (1)$$

Here E_x denotes the exact exchange energy, E_x^{PBE} is the PBE exchange, and E_c^{PBE} is the PBE correlation functional. E_x has the usual Hartree-Fock form in terms of one-electron orbitals. In the WSC method, this term is expressed in terms of localized Wannier orbitals $\{\tilde{\varphi}_i\}$. These are obtained through an unitary transformation of the delocalized Bloch states $\{\varphi_i\}$ corresponding to occupied bands. In particular, we use maximally localized Wannier functions (MLWFs)¹⁸, which are exponentially localized. In this way, a significant truncation in both number and size of exchange pairs can be achieved in real space.

We now turn to the calculation of the band gap. In extended insulating systems the band gap is simply given

by the difference between the eigenvalue of the highest occupied and the lowest empty state. Once the ground state has been minimized self-consistently, the eigenvalue of the empty state φ_e can be obtained through a simple non-selfconsistent calculation. With the hybrid PBE0 functional, the equation for φ_e is

$$\begin{aligned} & \left(-\frac{1}{2}\nabla^2 + V_{\text{ion}}(\mathbf{r}) + V_{\text{H}}[\rho^{\text{val}}(\mathbf{r})] + \frac{3}{4}V_x^{\text{PBE}}[\rho^{\text{val}}(\mathbf{r})] \right. \\ & \left. + V_c^{\text{PBE}}[\rho^{\text{val}}(\mathbf{r})] \right) \times \varphi_e(\mathbf{r}) + \frac{1}{4} \int V_x^{\text{val}}(\mathbf{r}, \mathbf{r}') \varphi_e(\mathbf{r}') d\mathbf{r}' \\ & = \varepsilon_e \varphi_e(\mathbf{r}), \end{aligned} \quad (2)$$

In the above expression we have assumed, for simplicity, a closed-shell system with $N/2$ doubly occupied one-electron states (extension to spin-polarized systems is straightforward); V_{H} and V_{ion} are the Hartree and the ionic (pseudo-)potentials, respectively; V_x^{PBE} and V_c^{PBE} are the PBE exchange and correlation potentials. We note that V_{H} , V_x^{PBE} and V_c^{PBE} are fixed operators as they only depend on the (fixed) valence charge density $\rho^{\text{val}}(\mathbf{r}) = \sum_j^{\text{occ}} \varphi_j^*(\mathbf{r}) \varphi_j(\mathbf{r})$. Finally, the non-local exact exchange potential $V_x^{\text{val}}(\mathbf{r}, \mathbf{r}')$ is given by:

$$V_x^{\text{val}}(\mathbf{r}, \mathbf{r}') = -2 \sum_j^{\text{occ}} \frac{\tilde{\varphi}_j^*(\mathbf{r}') \tilde{\varphi}_j(\mathbf{r})}{|\mathbf{r} - \mathbf{r}'|}, \quad (3)$$

where the sum runs over all the occupied states. This potential describes the exchange interaction between the empty state and each of the valence MLWFs $\{\tilde{\varphi}_j\}$.

The action of $V_x^{\text{val}}(\mathbf{r}, \mathbf{r}')$ on the empty state φ_e in Eq. (3) is given by:

$$\begin{aligned} D_x^e(\mathbf{r}) &= -2 \sum_j^{\text{occ}} \int d\mathbf{r}' \frac{\tilde{\varphi}_j^*(\mathbf{r}') \varphi_e(\mathbf{r}')}{|\mathbf{r} - \mathbf{r}'|} \times \tilde{\varphi}_j(\mathbf{r}) \\ &= -2 \sum_j^{\text{occ}} v_{ej}(\mathbf{r}) \tilde{\varphi}_j(\mathbf{r}) \end{aligned} \quad (4)$$

Here v_{ej} is the Coulomb potential originating from the “exchange charge” $\rho_{ej} = \tilde{\varphi}_j^*(\mathbf{r}') \varphi_e(\mathbf{r}')$, and satisfies the Poisson equation:

$$\nabla^2 v_{ej} = -4\pi \rho_{ej} \quad (5)$$

It is important to note that, while the empty eigenstate of Eq. (2) is Bloch like and delocalized in real space, the exchange pair density ρ_{ej} is confined by the valence MLWFs that are well localized in real space. As a result, the Poisson equation, Eq. (5), and the action of the exchange operator, Eq. (4), need only be solved in the region where $\tilde{\varphi}_j \neq 0$.

We have implemented the above computational procedure for calculating the PBE0 band gap in the CP code of the Quantum-ESPRESSO package.²⁰ The procedure works as a post processing feature following a PBE0 ground state calculation by the MLWF-based WSC method. In this work, we use it to calculate the electronic structure, particularly the band gap, of GaN,

InN, and $\text{In}_{1-x}\text{Ga}_x\text{N}$ in the zincblende phase. These systems are computationally challenging because InN and In-rich $\text{In}_{1-x}\text{Ga}_x\text{N}$ are incorrectly predicted to be metallic by standard GGA calculations.

The calculations were performed using a 64-atom cubic supercell to model both $\text{In}_{1-x}\text{Ga}_x\text{N}$ and its parent compounds, GaN and InN. For each Ga concentration x in the ternary $\text{In}_{1-x}\text{Ga}_x\text{N}$ compound, only a few selected atomic configurations were considered, with no specific treatment of disorder effects, as e.g. in Refs. 4,7; within our limited sampling, a very weak dependence of the calculated band gap on the specific cation arrangement was observed. For direct comparison with experiments and other theoretical results, the experimental lattice constants of GaN ($a = 4.50 \text{ \AA}$) and InN ($a = 4.98 \text{ \AA}$) were used, while the lattice parameter of the alloy was determined by linear interpolation.

TABLE I: Pseudopotential generation parameters. Here “ref.” refers to the reference state occupation, r_c refers to the cut-off radius, q_c is the cut-off wavevector and N_B is the number of Bessel functions used for each channel (see Ref. 28).

Atom	parameter	s	p	d
N	ref.	2.0	3.0	–
	r_c	1.30	1.30	–
	q_c	7.50	7.50	–
	N_B	10	10	–
Ga	ref.	2.0	1.0	10.0
	r_c	1.80	2.20	1.80
	q_c	8.00	8.00	8.36
	N_B	6	8	10
In	ref.	2.0	1.0	10.0
	r_c	1.90	2.30	1.80
	q_c	8.00	8.00	8.00
	N_B	8	8	8

Table I shows the reference states and cut-off radii used to construct the pseudopotentials used in this study. All pseudopotentials were generated using the OPIUM code²¹.

Unlike with traditional density functional theory, Hartree-Fock pseudopotentials require extra care in their construction. This arises from the non-local form of the Hartree-Fock exchange potential^{22,23,24,25}. The presence of the non-local exchange potential in Hartree-Fock or Hartree-Fock/DFT hybrids will often yield pseudopotentials with an unphysical, long-range tail. A correction procedure is necessary to remove this tail and restore the correct long-range behavior of the pseudopotential while maintaining the eigenvalue spectrum and logarithmic derivatives. Recent work^{22,26,27} has shown that this approach yields highly accurate Hartree-Fock pseudopotentials.

The pseudopotentials were norm-conserving/RRKJ type²⁸ and were generated from self-consistent PBE0 all-electron reference states using the approach of Ref. 27. The Ga and In pseudopotentials were obtained from scalar-relativistic solutions, while the N pseudopotential

was non-relativistic. The local potential was the s channel for all cases. The semi-core d electrons were treated as valence electrons in In and Ga (this corresponds to 576 valence electrons, *i.e.* 288 occupied states, in the 64-atom supercell). The plane-wave energy cutoff was 70 Ry and the Brillouin zone was sampled at the Γ point. Atomic positions in the supercell were relaxed at the GGA-PBE level.

The PBE0 ground state was determined by the WSC method, using MLWFs to calculate the exchange interaction among valence electrons¹⁴. While the MLWFs generated from the PBE ground state often give an excellent initial guess for the PBE0 calculations, for InN and In rich $\text{Ga}_x\text{In}_{1-x}\text{N}$ alloy configurations, the PBE ground state shows an incorrect ordering of the energy bands. For this reason, instead of PBE Wannier orbitals we used a set of fictitious localized orbitals at the guess bonding centers as the trial solutions for Eq. (2). This procedure was essential to obtain the PBE0 ground state with correct symmetry for InN and In rich $\text{Ga}_x\text{In}_{1-x}\text{N}$. In the empty state calculations, for each PBE0 ground state MLWF we first defined an orthorhombic box such that outside this box $\rho_{ej}(\mathbf{r})$ is smaller than a given cut-off value ρ^{cut} ; we take this cut-off equal to $2 \times 10^{-4} \text{ bohr}^{-3}$ in the present work. Then Eq. (5) is solved by the conjugate gradient method¹⁴, and for each pair ρ_{ej} formed by the empty state and a PBE0 ground state MLWF its action Eq. (4) is applied only inside the above truncated box. Finally with this $D_x^e(\mathbf{r})$, Eq. (2) is solved via a damped second order Car-Parrinello dynamics¹⁹.

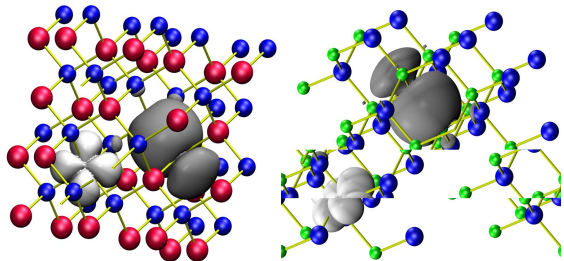


FIG. 1: (Color online.) Isosurfaces of typical d -like and sp^3 like Wannier orbitals in the InN (on the left) and GaN (on the right) 64-atom supercell. The Ga, In and N atoms are denoted by the green, red and blue spheres respectively.

Representative MLWFs for InN in its PBE0 ground state are shown in Fig. 1. Two types of valence MLWFs are present in our calculations, d -like Wannier orbitals centered at the In sites, and covalent sp^3 -like orbitals centered between the cations and the anions. As one can see from the figure, the d -like orbitals originating from the cation semi-core states are more localized than the sp^3 -like ones. The valence MLWFs are qualitatively similar for GaN, except for a slightly more pronounced localization related to the larger band gap.

The band structure properties of GaN and InN that result from our PBE0-MLWFs calculations are summa-

TABLE II: Valence band width, band gap and average d -band binding energy (eV) of GaN and InN.

		VBW	E_g	E_d
GaN	PBE0-MLWFs	17.70	3.52	-16.16
	PBE	16.14	1.60	-13.62
	PBE0, plane waves ^a	17.72	3.61	
	GW ^b		3.53	-16.5
	Experiment ^c		3.3	-17.7
InN	PBE0-MLWFs	17.04	1.09	-15.30
	PBE results	15.04	-0.04	-13.48
	GW ^b		0.78	-15.3
	Experiment		0.61 ^b	-16.0 ^c

^aReciprocal space method in PWSCF (Ref. 20) in 2-atom cell and $4 \times 4 \times 4$ k points

^bReference 29.

^cReference 30.

rized in Table II. Here we report the valence band width (VBW), the band gap E_g and the average d -band binding energy E_d , and compare them to PBE calculations (performed with the same 64-atom supercell used for the PBE0 calculations) and experimental results. For further comparison, we also report the results of PBE0 calculations performed using the reciprocal space implementation in Ref. 20; we can see that the agreement between these results and our MLWF-based calculations is very good. From Table II it appears that the GGA-PBE results significantly overestimate the energetic position of the cation d -bands. Because of the pd repulsion, the overestimated d bands level in turn pushes the p band upwards, resulting in an underestimated band gap. For InN, this effect leads to a wrong ordering of the Γ_{1c} and Γ_{15v} energy levels, and thus to the incorrect prediction of a metallic ground state. In the PBE0 calculations, the inclusion of exact exchange reduces the delocalization error. As shown by Table II, the PBE0 VBW is larger and the d -bands level shifts downwards, in better agreement with the experiment. In turn, this leads to a considerable improvement of the band gaps of both InN and GaN with respect to experiment; in particular, the PBE0 band gap becomes 1.09 eV for InN. It is also worth noticing that calculation of the PBE0 band gap using a PBE pseudopotential yields a ~ 0.2 eV smaller value than that obtained with the PBE0 pseudopotential.

Besides confirming the good performance of hybrid functionals for band gap predictions, the above results for InN and GaN provide evidence of the reliability of our procedure for calculating the PBE0 band gap. We have thus applied this procedure to the study of the ternary $\text{In}_{1-x}\text{Ga}_x\text{N}$ compound, a system for which the standard reciprocal space approach to calculate the exact exchange would be extremely cumbersome. Instead, our order- N scheme is well suited to treat systems for which large supercells are needed. Using a 64-atom supercell, we then considered $\text{In}_{1-x}\text{Ga}_x\text{N}$ models with 1(31), 2(30), 3(29), 4(28), 16(16), 28(4), 29(3), 30(2) and 31(1) Ga(In) cations, which correspond to $x = 0.031, 0.063, 0.094,$

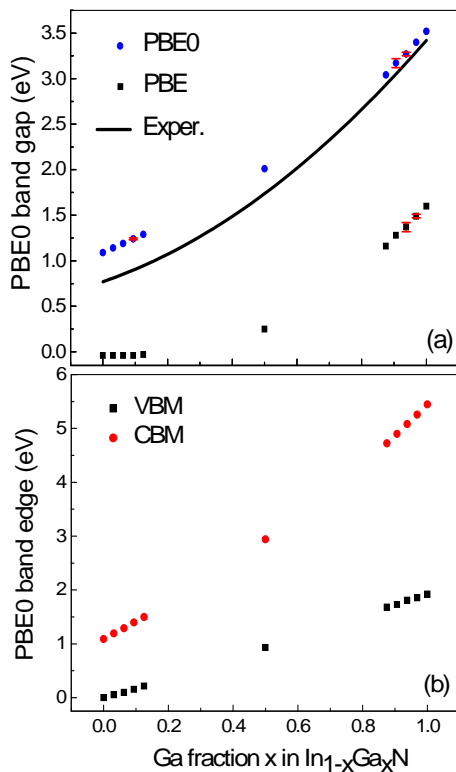


FIG. 2: (Color online.) (a) PBE0, PBE and experimental band gap of dependence Ga fraction x (b) Valence band maximum (VBM) and conduction band minimum as a function of Ga fraction x in $\text{In}_{1-x}\text{Ga}_x\text{N}$

0.125, 0.5, 0.875, 0.906, 0.938, and 0.969. For each value of x and a given configuration of Ga(In) atoms, the atomic positions were relaxed at the PBE level. The computed PBE0 band gap of $\text{In}_{1-x}\text{Ga}_x\text{N}$ as a function of the Ga fraction x is shown in Fig. 2(a), together with experimental³¹ and PBE results. We can see that PBE not only significantly underestimates the band gap but incorrectly shows a metallic ground state for $x < 0.5$. By contrast, a direct band gap at the Γ point is found for all values of x at the PBE0 level. Moreover, PBE0 predicts a large band gap bowing effect, in qualitative agreement with the experiment³¹. The band gap can be fitted to the quadratic form

$$E_g^{\text{alloy}} = xE_g^{\text{GaN}} + (1-x)E_g^{\text{InN}} - x(1-x)b \quad (6)$$

from which a bowing coefficient $b^{\text{PBE0}} = 1.63$ eV can be extracted, similar to the value, 1.67 eV, found in previous screened-exchange density functional (sx -LDA) calculations⁴. However, this is somewhat larger than the experimental value $b^{\text{expt}} = 1.43$ eV³¹, likely because of the overestimated PBE0 band gap for the In-rich compounds. To gain more insight into the origin of the large band gap bowing, we have examined how the valence band maximum (VBM) and conduction band minimum (CBM) depend separately on x , see Fig. 3(a). In this analysis, the average electrostatic potential was taken as

the reference for the band alignment. It can be seen that the VBM increases almost linearly with x , whereas the CBM shows a stronger nonlinear increase which is responsible for the large bowing coefficient of the alloy.

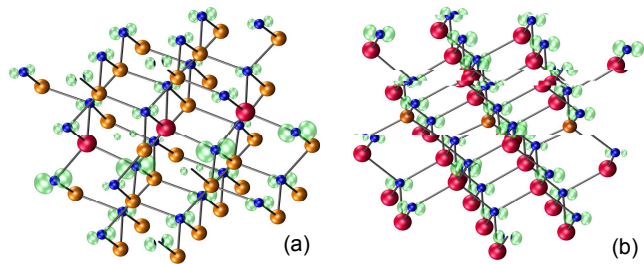


FIG. 3: (Color online.) Isosurfaces of PBE0 eigenstate (a) $\text{In}_3\text{Ga}_{29}\text{N}$ where 3 In atoms forms a zigzag chain structure; (b) $\text{Ga}_3\text{In}_{29}\text{N}$ where 3 Ga atoms forms a zigzag chain N atoms are denoted by red, orange and blue spheres respectively

The electronic states in proximity of the VBM are important for the photoluminescence properties of $\text{In}_{1-x}\text{Ga}_x\text{N}$. These states have the character of p orbitals localized at the N sites. Previous theoretical studies of $\text{In}_{1-x}\text{Ga}_x\text{N}$ found that in Ga-rich alloys the amplitude of these states is enhanced at N sites close to In impurities^{4,7}, suggesting a localization of photoexcited holes at such sites. This interesting result is confirmed by our PBE0 hybrid calculations. The enhancement, or hole localization, is particularly evident when the In impurities are clustered to form a zigzag In-N-In-N-In chain, as shown in Fig. 3(a). This localization has been suggested to be the reason of the high efficiency of $\text{In}_{1-x}\text{Ga}_x\text{N}$ based emitting devices^{4,6}. Interestingly, we found that there is an opposite effect for the case of Ga impurities in In rich alloys. Here, a reduction of the p states at the N sites along the Ga-N-Ga-N-Ga-N chain is observed, see Fig. 3(b).

In conclusion, we have described an efficient procedure to calculate the band gap of extended insulating systems using hybrid functionals. This procedure is based on the recently developed WSC order- N method, in which the Hartree Fock exchange is calculated using MLWFs, and can therefore be used to study the band gap and other electronic properties of systems with large unit cells. We have demonstrated the effectiveness of our approach by a study of the band gap of a ternary compound, $\text{In}_{1-x}\text{Ga}_x\text{N}$, that we have modeled using a 64-atom supercell. Hybrid functional results for this important material are here reported for the first time, without the approximation of screened exchange, and show a much better agreement with experiment than conventional DFT-GGA or LDA calculations. Our approach can be widely used for the band gap engineering problem in semiconductor alloys.

Acknowledgments

This work has been supported by the Department Of Energy under grant DE-FG02-06ER-46344, grant DE-

FG02-05ER46201 and by AFOSR-MURI F49620-03-1-0330. A. M. R. was supported by the (US) Department of Energy under grant DE-FG02-07ER46431

-
- ¹ P. Piquini, P. A. Graf, and A. Zunger, Phys. Rev. Lett. **100**, 186403 (2008). S. V. Dudiy and A. Zunger, *ibid* **97**, 046401 (2006).
- ² A. Grüneis, K. Hummer, M. Marsman, and G. Kresse, Phys. Rev. B **78**, 165103 (2008).
- ³ M. N. Huda, Y. Yan, S. -H. Wei, and M. M. Al-Jassim, Phys. Rev. B **78**, 195204 (2008).
- ⁴ B. Lee and L. -W. Wang, J. Appl. Phys. **100**, 093717 (2006).
- ⁵ J. W. Bennett, I. Grinberg, and A. M. Rappe, J. Am. Chem. Soc. **130**, 17409 (2008).
- ⁶ S. F. Chichibu *et al.*, Philos. Mag. **87**, 2019 (2007).
- ⁷ L. Bellaiche, T. Mattila, L. -W. Wang, S. -H. Wei, and A. Zunger, Appl. Phys. Lett. **74**, 1842(1999).
- ⁸ See e.g. R. G. Parr and W. Yang, *Density Functional Theory of Atoms and Molecules* (Oxford University Press, New York, 1989).
- ⁹ A. J. Cohen, P. Mori-Sanchez, and W. Yang, Science **321**, 792 (2008).
- ¹⁰ A. J. Cohen, P. Mori-Sanchez, and W. Yang, Phys. Rev. B **77**, 115123 (2008).
- ¹¹ B. G. Janesko, T. M. Henderson, and G. E. Scuseria, Phys. Chem. Chem. Phys., **11**, 443 (2009).
- ¹² A. D. Becke, J. Chem. Phys. **98**, 1372 (1993).
- ¹³ M. Marsman, J. Paier, A. Stroppa, and G. Kresse, J. Phys.: Condens. Matter **20**, 064201 (2008).
- ¹⁴ X. Wu, A. Selloni, and R. Car, Phys. Rev. B **79**, 085102 (2009).
- ¹⁵ N. Marzari and D. Vanderbilt, Phys. Rev. B **56**, 12847 (1997).
- ¹⁶ J. P. Perdew, M. Ernzerhof, and K. Burke, J. Chem. Phys. **105**, 9982 (1996).
- ¹⁷ J. P. Perdew, K. Burke, and M. Ernzerhof, Phys. Rev. Lett. **77**, 3865 (1996).
- ¹⁸ N. Marzari and D. Vanderbilt, Phys. Rev. B **56**, 12847 (1997).
- ¹⁹ R. Car, in *Conceptual Foundations of Materials: A Standard Model for Ground- and Excited-State Properties, Contemporary Concepts of Condensed Matter Science*, edited by S. G. Louie and M. L. Cohen (Elsevier, Amsterdam, 2006), Chap. 3, p. 64.
- ²⁰ See <http://www.quantum-espresso.org>.
- ²¹ OPIUM pseudopotential package <http://opium.sourceforge.net>.
- ²² J. R. Trail and R. J. Needs, J. Chem. Phys. **122**, 014112 (2005).
- ²³ D. M. Bylander and L. Kleinman, Phys. Rev. Lett. **74**, 3660 (1995); Phys. Rev. B **52**, 14566 (1995); **54**, 7891 (1996); **55**, 9432 (1997).
- ²⁴ M. Städele, J. A. Majewski, P. Vogl, and A. Görling, Phys. Rev. Lett. **79**, 2089 (1997).
- ²⁵ E. Engel, A. Höck, R. N. Schmid, R. M. Dreizler, and N. Chetty, Phys. Rev. B **64**, 125111 (2001).
- ²⁶ J. R. Trail and R. J. Needs, J. Chem. Phys. **122**, 174109 (2005).
- ²⁷ W. A. Al-Saidi, E. J. Walter, and A. M. Rappe, Phys. Rev. B **77**, 075112 (2008).
- ²⁸ A. M. Rappe, K. M. Rabe, E. Kaxiras, and J. D. Joannopoulos, Phys. Rev. B **41**, R1227 (1990).
- ²⁹ F. Fuchs, J. Furthmüller, F. Bechstedt, M. Shishkin, and G. Kresse, Phys. Rev. B **76**, 115109 (2007).
- ³⁰ L. F. J. Piper, T. D. Veal, P. H. Jefferson, C. F. McConville, F. Fuchs, J. Furthmüller, F. Bechstedt, H. Lu and W. J. Schaff, Phys. Rev. B **72**, 245319 (2005).
- ³¹ J. Wu, W. Walukiewicz, K. M. Yu, J. W. Ager III, E. E. Haller, H. Lu, and W. J. Schaff, Appl. Phys. Lett. **80**, 4741 (2002).